PROGRESS IN PHOTOVOLTAICS: RESEARCH AND APPLICATIONS
Prog. Photovolt: Res. Appl. 2009; **17**:394–402
Published online 28 April 2009 in Wiley InterScience (www.interscience.wiley.com) DOI: 10.1002/pip.895

Research

Reciprocity Between Electroluminescence and Quantum Efficiency Used for the Characterization of Silicon Solar Cells

Thomas Kirchartz[1*,†], Anke Helbig[2], Wilfried Reetz[1], Michael Reuter[2], Jürgen H. Werner[2] and Uwe Rau[1]
[1]*IEF5-Photovoltaik, Forschungszentrum Jülich, 52425 Jülich, Germany*
[2]*Institut für Physikalische Elektronik, Universität Stuttgart, 70569 Stuttgart, Germany*

Spectrally and spatially resolved electroluminescence emission of crystalline silicon solar cells is interpreted in terms of two electro-optical reciprocity relations. The first relation links the photovoltaic quantum efficiency to the electroluminescence spectrum. Both methods contain information on recombination and the optical pathlength of the incident light, simultaneously. From the electroluminescence spectrum, we derive the pathlength enhancement factor of textured and untextured crystalline silicon solar cells. Further, we use local quantum efficiency measurements to quantitatively explain light induced current as well as panchromatic electroluminescence images. A second reciprocity relation connects open circuit voltage of a solar cell with the light emitting diode quantum efficiency of the same device. For a given quality of light trapping and a given open circuit voltage, we predict the attainable LED quantum efficiency and verify our results experimentally. Copyright © 2009 John Wiley & Sons, Ltd.

KEY WORDS: luminescence; reciprocity; LED; quantum efficiency

Received 11 September 2008; Revised 12 February 2009

INTRODUCTION

Luminescence imaging has become a valuable tool for solar cell characterization due to the short measurement time and its sensitivity to various detrimental effects like shunts, increased resistances and recombination. If excess carriers are generated optically and the photoluminescence is detected,[1] the measurement is contactless and applicable at all steps in the production process. In contrast, electroluminescence (EL)[2] applies to solar cells, modules or systems with external contacts for current injection. The necessary equipment consists of a Si CCD camera and a current supply, capable of delivering the required current densities of the order of 50 mA/cm^2. The detected luminescence image reveals those regions on the device being most detrimental to the total performance. However, since luminescence imaging contains information about optical, electronic and resistive effects all intermixed, it is rather difficult to identify the specific origin for local variations of the luminescence.

The present paper shows that the analysis of spectrally and spatially resolved EL of solar cells quantitatively relies on the opto-electronic reciprocity between the photovoltaic and the electroluminescent action[3] of these devices. The key to both interpretation and simulation of EL spectra is contained in a single equation relating the

*Correspondence to: Thomas Kirchartz, IEF5-Photovoltaik, Forschungszentrum Jülich, 52425 Jülich, Germany
†E-mail: t.kirchartz@fz-juelich.de

electroluminescence emission with the photovoltaic quantum efficiency. Recent attempts to model the EL emission consider the effect of the minority carrier distribution[4] and the reabsorption of photons[5] on the emitted spectrum. Both effects influence the spectral solar cell quantum efficiency in a way that is complementary to their influence on the EL spectrum. As both spectra are interlinked by reciprocity, the challenge of interpreting the EL emission is reduced to the task of interpreting the quantum efficiency, where a series of well-established solutions is readily available. Modelling of EL emission can be therefore replaced by computation of the quantum efficiency either analytically or numerically. Note that the proposed approach of linking the quantum efficiency to the EL emission is fully compatible with the approach of modelling the minority carrier distribution combined with an appropriate reabsorption scheme.[6]

Figure 1 sketches the device with optical and electrical terminals. Figure 1a shows the situation, where the device operates as a light emitting diode (LED), i.e., the device is excited electrically leading to an optical output signal. If operated as a solar cell, only the direction of the arrows has to be reversed; the excitation is optical and the output is electrical as shown in Figure 1b. In both cases, the essential question is the reciprocal connection between the input and output terminals, i.e., the quantity describing the characteristics of the device that influence both the generation of a photocurrent as well as the emission of photons. These quantities connecting input and output terminals are the external solar cell quantum efficiency Q_e and the internally applied voltage V at the collecting junction, no matter whether we convert light into electrical energy or vice versa. Figure 1c sketches a spatially extended device, which absorbs and emits light at different position of its surface. In general, the device properties at each position may be different. Thus, Figure 1c describes the device as a parallel connection of diodes connected by a network of resistances. Every diode has its own local quantum efficiency and its own local junction voltage, which determine the local EL emission a CCD camera would detect.

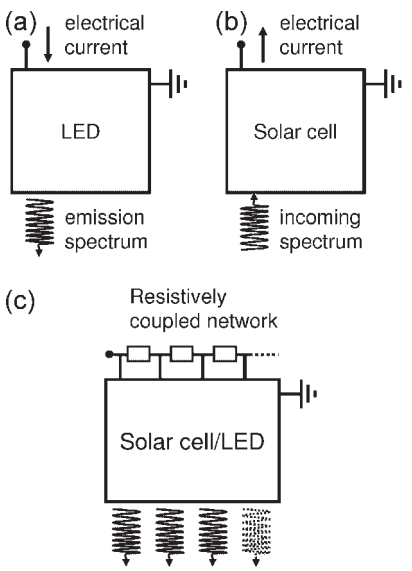

Figure 1. Sketch of an (a) LED and (b) solar cell with optical and electrical terminals. Both devices are identical except for the direction of the arrows denoting excitation and response to the excitation. (c) Sketch of a spatially extended device, which absorbs and emits light at different position of its surface. The device is built up of a parallel connection of diodes connected by a network of resistances. Every diode has its own local quantum efficiency and its own local junction voltage, which determine the local EL emission a CCD camera would detect

THEORY

At any coordinate $\mathbf{x} = (x, y)$ of the surface of the solar cell, its electroluminescent emission—quantified in terms of a local excess photon density $\phi_{em}(E,\mathbf{x})$—and its local external quantum efficiency $Q_e(x)$ are interlinked by the spectral reciprocity theorem of Reference 3. The excess photon density $\phi_{em}(E,\mathbf{x})$ emitted by a solar cell at photon energy E and surface coordinate $\mathbf{x}$ under voltage bias V is given by:[3,7–9]

$$\phi_{em}(E,x) = [1 - R(E,x)]Q_i(E,x)\phi_{bb}(E) \times \left[\exp\left(\frac{qV(x)}{kT}\right) - 1\right] \quad (1)$$

where kT/q is the thermal voltage, R the reflectance of the cell's surface, $Q_i(E,x) = [1 - R(E,x)]^{-1}Q_e(E,x)$ the cell's internal quantum efficiency and

$$\phi_{bb}(E) = \frac{2\pi E^2/(h^3c^2)}{\exp(E/kT) - 1} \approx \frac{2\pi E^2}{h^3c^2}\exp\left\{\frac{-E}{kT}\right\} \quad (2)$$

the spectral photon density of a black body. Here, h is Planck's constant and c the vacuum speed of light. Note that here and in the following we consider the incidence of light as well as the emission of light only perpendicular to the cell's surface though Equation (1) is valid for any angle of incidence and emission.

DOI: 10.1002/pip

It is interesting to note that in Equation (1) the dependence of $\phi_{em}(E,\mathbf{x})$ on the coordinate $\mathbf{x}$ shows up in (i) the reflectance $R(E,\mathbf{x})$, (ii) in the local internal quantum efficiency $Q_i(E,\mathbf{x})$, and (iii) in the local junction voltage $V(\mathbf{x})$ that might be different at different coordinates along the junction area. Thus, the three different terms in Equation (1) to a first order approximation correspond to the classical loss mechanisms in solar cells: (i) optical losses, (ii) recombination losses, and (iii) resistive losses.[10]

SPECTRALLY RESOLVED ELECTROLUMINESCENCE

We measure the EL of mono-crystalline silicon solar cells with a liquid nitrogen cooled Ge-detector attached to a single stage monochromator. The emitter layers of all samples are formed via $POCl_3$ diffusion followed by a drive-in process step. The front contacts consist of an evaporated TiPdAg alloy. The back surface is passivated either with a-Si:H or SiO_2. A function generator applies a rectangularly shaped voltage to the sample and a lock-in amplifier amplifies the signal of the Ge-detector. Figure 2 shows the detected room temperature EL (full circles) of a textured sample in arbitrary units. By applying Equation (1), we determine the external quantum efficiency $Q_{e,EL}$ (full triangles) in arbitrary units that follows from the EL spectrum. A calibrated quantum efficiency measurement $Q_{e,dir}$ (open squares) allows to adjust the $Q_{e,EL}$ in the overlap region. Combining two totally different measurements, we finally receive a quantum efficiency spanning nine orders of magnitude (for five orders of magnitude of the EL emission) and revealing a good agreement of both measurements ($Q_{e,dir} \approx Q_{e,EL}$) in the overlap region.

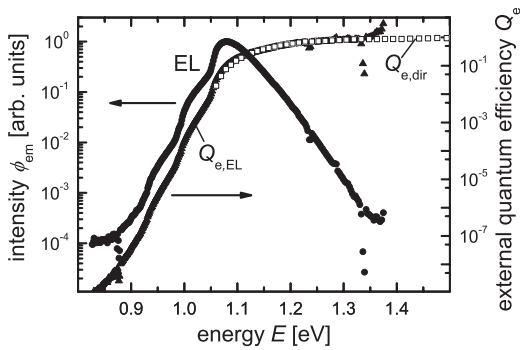

Figure 2. Electroluminescence spectrum, external quantum efficiency calculated from the EL spectrum, and directly measured quantum efficiency $Q_{e,dir}$ as a function of the photon energy. The quantum efficiency from EL is scaled to the directly measured $Q_{e,dir}$. The increased signal of the EL for energies $E > 1{\cdot}35$ eV is due to stray light

In principle, it is possible to extract parameters like the effective diffusion length L_{eff} from the EL measurement, as it is a standard procedure for quantum efficiency measurements. The spectral region substantial for the determination of L_{eff}, however, covers penetration depths $w_e \ll L_\alpha < w/4$, where w is the cell thickness and $w_e \approx 1\,\mu$m the emitter thickness. For cell thicknesses $w = 250\,\mu$m, this inequality corresponds approximately to an energy range $1{\cdot}31\,\text{eV} < E < 1{\cdot}59\,\text{eV}$, where luminescence emission is already much lower than it is at the peak. Stray light does not allow for a correct evaluation of the EL spectrum with our setup, as can be seen in Figure 2, featuring an additional signal due to stray light starting at around 1·35 eV. Thus, future investigations using a double stage monochromator for enhanced stray light suppression will allow more detailed investigation of the high energy part of the EL spectrum.

The electronic properties of the device affect mainly the high energy part of the EL spectrum, i.e., the same region that is usually used for the determination of the effective diffusion length from the internal quantum efficiency. In contrast, optical properties of the device are visible in the low energy regime, where the absorption length is much larger than the cell thickness. For these energies, photons are reflected multiple times at the internal surfaces before they generate electron/hole pairs, which contribute to the photocurrent. Thus, EL spectra nicely reveal the effect of increased light trapping, in crystalline silicon cells usually caused by textured front surfaces and highly reflective back surfaces. In order to quantify the quality of light trapping in our samples with EL, we need a useful mathematical description for the low energy part of the quantum efficiency. For weakly absorbed light ($\lambda > 1150$ nm) the generation rate $g(z) = (1 - R_f)\alpha\exp$ $\exp(-\alpha k_{eff} z)$ is virtually homogeneous over the depth of the device. Mathematically the homogeneity of the generation rate corresponds to a Taylor series of the generation rate for $\alpha z \approx 0$ which yields $g(z) \approx (1 - R_f)$ $\alpha k_{eff} z_{.w}$ Finally, the external quantum efficiency $Q_e = \int_0 f_c(z) g(z) \mathrm{d}z$ becomes:

$$Q_e = (1 - R_f)\alpha k_{eff} \int_0^w f_c(z)\mathrm{d}z \qquad (3)$$

DOI: 10.1002/pip

and, thus, proportional to the absorption coefficient α times an effective pathlength enhancement factor k_{eff}. The pathlength enhancement k_{eff} describes the path weakly absorbed light travels in the cell before it leaves the cell as a multiple of the cell thickness. Summarized in the quantity k_{eff} are the properties of the front texture, which diffracts light into oblique angles, and the quality of the back reflector. In Equation (3), R_{f} denotes the reflectance at the front surface, while $f_{\text{c}}(z)$ is the collection efficiency of photogenerated carriers.

Since photogeneration is homogeneous for low absorption, we use the average collection efficiency

$$\overline{f}_c = \frac{1}{w}\int_0^w f_{\text{c}}(z)\text{d}z = \frac{L}{w}\frac{S(\cos\, h(w/L) - 1) + D/L \sin\, h(w/L)}{S \sin\, h(w/L) + D/L \cos\, h(w/L)} \quad (4)$$

which we calculate from the dark carrier distribution, using Donolato's theorem [11]. The average collection efficiency depends on the bulk diffusion length L, the diffusion coefficient D, and the back surface recombination velocity S. From Equation (3) now follows the pathlength enhancement as:

$$k_{\text{eff}} = \lim_{\alpha\to 0}\frac{Q_{\text{e}}}{\alpha w \overline{f}_c(1 - R_{\text{f}})} \quad (5)$$

Figure 3 shows the result of plotting $k_{\text{eff}} = Q_{\text{e}}/(\overline{f}_c \alpha w(1 - R_{\text{f}}))$ as a function of the absorption coefficient.

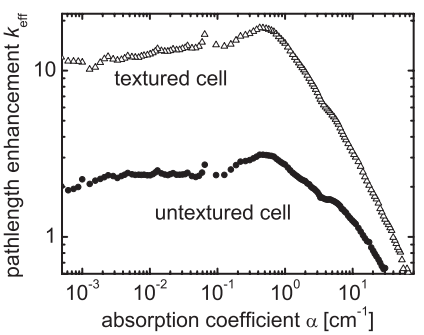

Figure 3. Comparison of the pathlength enhancement factor k_{eff} as a function of the absorption coefficient for two different samples, one with a random texture and one without texture, shows the strong increase of the average pathlength for the sample with surface texture compared to the flat sample. The pathlength enhancement follows from the data only in the limit of low absorption coefficients, while for high absorption coefficients the data goes below unity meaning that all photons are absorbed before they reach the back contact for the first time

The front surface reflection was measured and extrapolated linearly into the infrared, since the measured signal in the infrared is affected by light that has been reflected internally multiple times. The collection efficiency used for these results was calculated assuming a high diffusion length $L = 2$ mm appropriate for these mono-crystalline floatzone cells, a surface recombination velocity of $S = 100$ cm/s and an electron diffusion constant $D = 27\,\text{cm}^2/\text{s}$ (corresponding to a doping concentration $N_{\text{A}} = 10^{16}\,\text{cm}^{-3}$). The diffusion length L is estimated to be of the same order of magnitude but slightly below the Auger limit, which is $L \approx 4$ mm.[12] The values for the collection efficiency are then $\overline{f}_c = 0.90$ for the 550 μm thick untextured cell and $\overline{f}_{\text{c}} = 0.95$ for the 250 μm thick textured cell. Note that the pathlength enhancement in Figure 3 has to be taken for small absorption coefficients, where it saturates. For high absorption coefficients, the light is absorbed before it reaches the back side of the absorber and thus, the influence of light trapping on the spectrum vanishes and the value of $Q_{\text{e}}/(\overline{f}_{\text{c}}\alpha w(1 - R_{\text{f}}))$ is below unity. In this case of low wavelengths $\lambda < 1150$ nm and high absorption coefficients $\alpha > 1\,\text{cm}^{-1}$, the assumption that light is weakly absorbed is violated and the pathlength enhancement $k_{\text{eff}} \neq Q_{\text{e}}/(\overline{f}_{\text{c}}\alpha w(1 - R_{\text{f}}))$.

Figure 3 displays the results for a textured and an untextured mono-crystalline solar cell to demonstrate the effect of random pyramids obtained by a KOH etch. The textured cell with random pyramids has a pathlength enhancement $k_{\text{eff}} \approx 12$, which is due to the scattering of light in oblique angles, which are subsequently trapped inside the absorber due to total internal reflection. In contrast, the nominally flat solar cell has a pathlength enhancement of around $k_{\text{eff}} \approx 2$, since light is hardly scattered in oblique angles by the flat surfaces. Although the effect of the texture is clearly visible, the resulting value of $k_{\text{eff}} \approx 12$ is still much lower than the maximum possible value of $k_{\text{eff}} = 4n^2 \approx 50$,[13] where $n \approx 3{\cdot}5$ is the refractive index of silicon.

Note that the average pathlength enhancement as defined in Equation (5) is not necessarily a good measure for the increase of the photocurrent. As shown by Brendel,[14] not only a high *average* pathlength is important for increased photocurrent but also the distribution of pathlengths. A very sharp distribution of pathlengths, i.e., all pathlengths are nearly equal to the average pathlength, is more beneficial than a broad distribution. However, only the average pathlength is measured by our method shown in Figure 3 and not the also relevant distribution of pathlengths.

DOI: 10.1002/pip

SPATIALLY RESOLVED ELECTROLUMINESCENCE

Since solar cells are thin (~200 μm for wafer based silicon) but large area devices, spatial inhomogeneities and their characterization are of high importance for photovoltaics. The simplest approach to spatially resolved measurements is to measure the quantum efficiency two-dimensionally. However, recording the spectrum for each point on a cell would be extremely time-consuming. Thus, a common method, the so-called Light Beam Induced Current (LBIC) measurement, uses only a few different wavelengths of laser diodes or light emitting diodes. These nearly monochromatic light sources induce a certain short circuit current which is measured while scanning the cell with the light spot. In the following, this LBIC measurement will be compared to electroluminescence imaging.

Figure 4a shows an LBIC scan (10 mm × 10 mm) of a mono-crystalline silicon solar cell with a step size of 50 μm and with an LED with $\lambda \approx 950$ nm and approximately 0·1 suns intensity used as the radiation source. The LBIC scan clearly reveals a horizontal band with a lower LBIC signal. This feature stems from the Al being directly in contact with the silicon base while the rest of the back surface is passivated with thermally grown SiO_2. The contacts through the SiO_2 are realized through lithographically defined point contacts, which are also visible in the LBIC scan as small spots with decreased signal. This sample has the advantage of providing macroscopic regions of different back surface recombination velocity on the same cell. Those parts of the cell, where the back surface of the absorber is in direct contact with the metal, have a rather high surface recombination velocity and thus a decreased quantum efficiency and EL, while the parts passivated with SiO_2 have a lower surface recombination velocity and thus an increased quantum efficiency and thus also an increased LBIC signal. In the following, we will refer to the regions, where the metal is in direct contact with the absorber as the ''unpassivated regions'' (the point contacts and the dark horizontal band in Figure 4), and we will refer to the parts of the absorber, where the Si is in contact with the SiO_2 layer, as the ''passivated'' region.

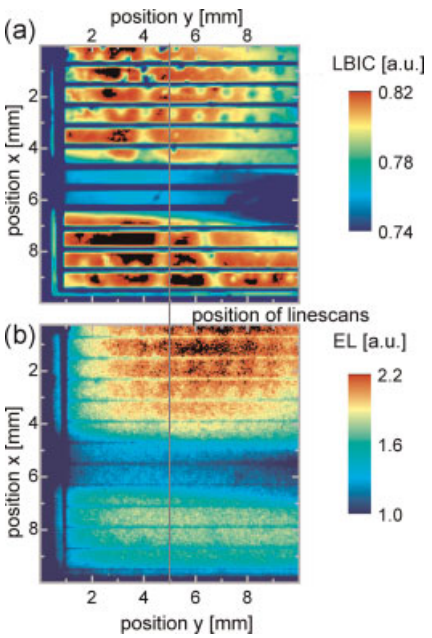

Figure 4. Comparison of (a) an LBIC scan (excitation wavelength $\lambda = 950$ nm) and (b) EL image of one part of a mono-crystalline silicon solar cell with different back surfaces. The dark horizontal band in both images stems from an unpassivated metal surface (high back surface recombination velocity S), while the rest of the back is passivated (small back surface recombination velocity S) with a SiO_2 layer with small point contacts. The y-position, which is later used for the linescans in Figure 6, is indicated by a vertical line

Figure 4b shows the corresponding EL image of the same region on the solar cell. The image is taken with an injection current $J_{inj} = 7{\cdot}5\,mA\,cm^{-2}$ (cell size: $4\,cm^2$) and an integration time of 300 s. Qualitatively, the image looks very similar to the LBIC image. However, superimposed to the intensity variation between the passivated and unpassivated regions due to different surface recombination is an intensity variation depending on the distance to the contact located in the upper left corner of the image. This additional feature arises because the internal voltage decreases with increasing distance from the contacts due to resistive voltage losses of the emitter and gridfingers.

In order to explain, in which way both images depend quantitatively on the local solar cell quantum efficiency $Q_e(\mathbf{x})$, we perform a series of quantum efficiency measurements at different positions close to the transition region between passivated and unpassivated back side. Theoretically, the quantum efficiency $Q_e(\mathbf{x}, \lambda \approx 950\,nm)$ should be proportional to the LBIC intensity values I_{LBIC}, i.e.,

$$I_{LBIC}(E,x) \propto Q_e(E,x) \tag{6}$$

Since our LBIC measurement setup has no absolute calibration, we have to use the proportionality sign in Equation (6), while for a calibrated setup

DOI: 10.1002/pip

$I_{\mathrm{LBIC}}(E,x) = Q_{\mathrm{e}}(E,x)$. For the EL measurement, the photon flux emitted by the solar cell is given by Equation (1), while the spectrally resolved intensity ϕ_{cam} of the camera signal is then:

$$\phi_{\mathrm{cam}}(E,x) \propto Q_{\mathrm{e}}(E,x)\phi_{\mathrm{bb}}(E)Q_{\mathrm{cam}}(E) \tag{7}$$

where Q_{cam} is the quantum efficiency of the camera. Of course, a varying local voltage $V(\mathbf{x})$ also influences the intensity ϕ_{cam} of the camera signal according to Equation (1), thereby making the quantitative interpretation more difficult. The EL image as shown in Figure 4b is a scalar value for each pixel. The intensity of the camera signal Φ_{cam} follows from Equation (7) via integration over energy, i.e.

$$\Phi_{\mathrm{cam}}(x) = \int \phi_{\mathrm{cam}}(E,x)\mathrm{d}E \tag{8}$$

Figure 5 shows the result of performing the operation in Equation (7) on the two quantum efficiency spectra. The solid lines represent both, the external quantum efficiency Q_{e}, as well as the spectrally resolved EL signal $\phi_{\mathrm{cam}}(E)$ from the camera for the measurement on the passivated region, while the dashed lines represent the same two quantities for the measurement on the unpassivated back side. The integral over the resulting curves for $\phi_{\mathrm{cam}}(E)$ then gives the camera signal Φ_{cam} under the assumption that the voltage does not vary locally.

In order to check, whether the above stated proportionalities (Equations (6) and (7)) really hold in experiment, we evaluate line scans of the LBIC and the EL image in Figure 4 and compare those with the quantum efficiencies $Q_{\mathrm{e}}(x, \lambda = 950\,\mathrm{nm})$ and the camera signals Φ_{cam} calculated from the quantum efficiency according to Equations (7) and (8).

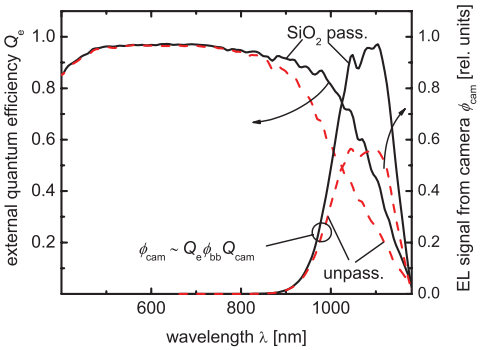

Figure 5. Quantum efficiency measured on the unpassivated region (the dark band in Figure 4; dashed lines) and on the passivated region (solid lines) and the resulting wavelength resolved intensity of the camera signal, calculated with Equation (6) and normalized to the peak of the spectra on the passivated region

Figure 6a shows the comparison between the LBIC linescan and quantum efficiencies taken at different positions and with different spot sizes. We made two sets of measurements, where we varied the x-coordinate in order to get quantum efficiency measurements on the passivated and unpassivated region, while keeping the y-coordinate constant at $y \approx 5$ mm. The two sets of measurements are distinguished by different symbols that indicate different spot sizes (squares: 1 mm × 3 mm; circles, triangles: 2 mm × 5 mm). Each quantum efficiency measurement corresponds to one symbol in Figure 6a and one symbol in Figure 6b.

From Equation (6), we would expect perfect agreement between LBIC intensity I_{LBIC} (950 nm) and quantum efficiency Q_{e} (950 nm). Figure 6a shows a decent agreement, although the difference between the quantum efficiency Q_{e} (950 nm) measurements on the passivated and the unpassivated regions seems to be higher than those of the LBIC linescan I_{LBIC} (950 nm).

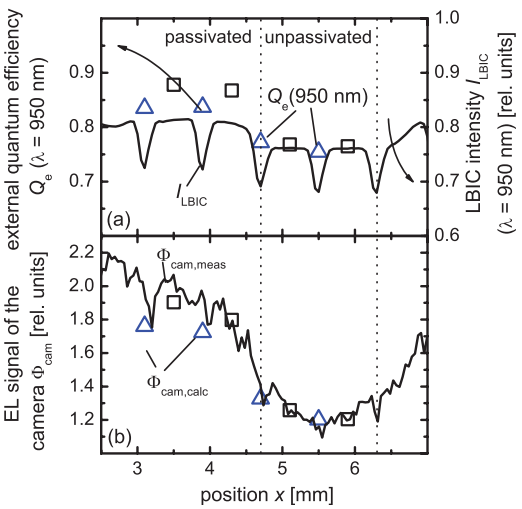

Figure 6. (a) Comparison of LBIC linescan of the image in Figure 4a with quantum efficiencies taken at 950 nm. (b) Comparison of the linescan of the EL image in Figure 4b with EL intensities calculated from quantum efficiency measurements as shown in Figure 5 showing an excellent agreement between the values calculated from the quantum efficiency and the values taken from the EL image. The y-position of both linescans is indicated by the vertical line in Figure 4 ($y \approx 5$ mm). The quantum efficiencies are also taken at $y \approx 5$ mm and with different spot sizes (squares: 1 mm × 3 mm; triangles: 2 mm × 5 mm)

DOI: 10.1002/pip

Figure 6b shows the EL linescan compared with the values calculated from the same quantum efficiency measurements as used for comparison with the LBIC. Now, we have to consider that there is a superposition of the effects of the quantum efficiency and the internal voltage on the shape of the EL-linescan as follows from Equation (1). Low values of x are equivalent to low distances from the contact, which is situated roughly at $x = 0$. Thus, for increasing x, the intensity of the EL signal goes down considerably even for constant Q_e. Considering this fact, Figure 6b shows a quite good correspondence between the values $\Phi_{cam,calc}(\mathbf{x})$ calculated according to the reciprocity relation between EL and quantum efficiency and the measured EL intensity $\Phi_{cam,meas}(\mathbf{x})$.

Thus, we have shown that the reciprocity relation (Equation (1)) is not only of relevance for spectrally resolved EL measurements but also describes EL images qualitatively very well. However, this finding does not immediately lead to a good method to quantify cell parameters in a spatially resolved way. Due to the intermixing of different influences in an EL image, quantitative interpretation of data and, thus, determination of more than one unknown, always requires an increase of the number of equations. This has been done to get access to the diffusion length[5] and to the series resistance,[15] while the reciprocity helps us to better interpret the results.[16]

ABSOLUTE EL EMISSION—LED QUANTUM EFFICIENCY

The photovoltaic quantum efficiency Q_e is a spectral quantity that defines the spectral response of a solar cell as well as the EL emission of a pn-junction diode via Equation (1). In contrast, the LED quantum efficiency, Q_{LED}, is a single number with a completely different definition than the photovoltaic quantum efficiency that has been used in Equation (1) for the calculation of the EL emission. The LED quantum efficiency relates the radiative and the non-radiative current via

$$Q_{LED}(V) = \frac{J_{rad}(V)}{J_{nr}(V) + J_{rad}(V)} \tag{9}$$

Note that we define the radiative recombination current as the electrical current leading to radiative recombination *and* escape of photons. The current that leads to radiative recombination, where the photon is reabsorbed and the created electron/hole pair then recombines non-radiatively, is also counted as non-radiative recombination current. The LED quantum efficiency depends on the open circuit voltage according to a second reciprocity theorem [7,8]

$$\Delta V_{OC} = V_{OC}^{rad} - V_{OC} = -\frac{kT}{q}\ln(Q_{LED}) \tag{10}$$

where the radiative open circuit voltage V_{OC}^{rad} follows solely from the solar cell quantum efficiency Q_e as:

$$\begin{aligned} V_{OC}^{rad} &= \frac{kT}{q}\ln\left(\frac{J_{sc}}{J_{0,rad}} + 1\right) \\ &\approx \frac{kT}{q}\ln\left(\int_0^\infty Q_e\phi_{sun}\mathrm{d}E \Big/ \int_0^\infty Q_e\phi_{bb}\mathrm{d}E\right) \end{aligned} \tag{11}$$

The link between the radiative saturation current density $J_{0,rad}$ and the solar cell quantum efficiency directly results from the spectral reciprocity, Equation (1), if one considers that the radiative recombination current must equal—as a particle current—the emission of light from the solar cell under applied bias, i.e., $J_{0,rad}/q = \phi_{em}/(\exp(qV/kT) - 1)$.

To predict the LED performance from solar cell properties, we need the actual V_{OC} and the radiative open circuit voltage V_{OC}^{rad}. For high quality silicon solar cells, the pathlength enhancement k_{eff} is the most important factor determining the quantum efficiency around the band gap and thus the radiative recombination current density J_{rad} and the radiative open circuit voltage V_{OC}^{rad}. We therefore approximate the solar cell quantum efficiency by the absorptance[17,18]

$$a(E) = \frac{1}{\left(1 + \frac{1}{\alpha k_{eff} w}\right)} \tag{12}$$

using an approximation for textured surfaces. Inserting the absorptance defined by Equation (12) instead of the solar cell quantum efficiency into Equation (11) leads to a radiative open circuit voltage $V_{OC}^{rad}(k_{eff})$ as a function of the light trapping properties. Subsequently, we measure both open circuit voltages and LED quantum efficiencies of several textured mono-crystalline solar cells and compared them to the predictions for different pathlength enhancement factors.

Figure 7 shows the comparison between experiment (symbols) and theory (lines). The high quality samples are all within the typical range of $10 < k_{eff} < 20$ that corresponds to our investigations with the EL spectra. Thus, the results presented in Figures 3 and 7 are not

DOI: 10.1002/pip

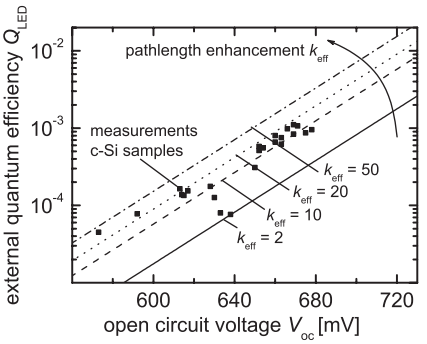

Figure 7. External LED quantum efficiency as a function of the open circuit voltage. The measurements (squares) of randomly textured mono-crystalline silicon solar cells are compared with the predictions (lines) for different pathlength enhancement factors k_{eff}. Most of the devices with higher V_{oc} correspond to the theoretical prediction when pathlength enhancement factors $10 < k_{eff} < 20$ are assumed. This is agreement with the finding of Figure 3, where the presented randomly textured device had a $k_{eff} \approx 12$

contradictory, although the difficulty of measuring absolute intensities leads to a high degree of uncertainty for the results of Figure 7. Some of the lower quality samples seem to have even better light trapping. However, this effect is caused by strongly decreased quantum efficiencies, implying that our initial assumption $Q_e(E) = a(E)$ is no longer valid. Overestimations of the solar cell quantum efficiencies thus lead to underestimations of the radiative open circuit voltages and consequently to overestimations of the LED quantum efficiencies.

Figure 7 also shows which LED quantum efficiencies can be reached with solar cell technology. The crystalline silicon solar cells with the highest open circuit voltages $V_{oc} = 712\,\text{mV}$[19] are the HIT cells from Sanyo. According to the calculations in Figure 7, solar cells with such a V_{oc} and a perfect light trapping scheme approaching the Yablonovitch limit of $k_{eff} = 4n^2 \approx 50$[13] have the potential to reach a quantum efficiency of $Q_{LED} = 1{\cdot}3\%$, which is only slightly higher than the values reached by Green *et al.*[20]

SUMMARY

We have applied two reciprocity relations (Equations (1) and (10)) between the two optoelectronic applications of a diode—the light emitting diode and the solar cell. These reciprocity relations allow us to interpret the spectrally resolved, spatially resolved and the absolute intensity of the electroluminescent emission. Using EL spectra, we have shown how to quantify the pathlength enhancement as a quality factor for the light trapping. We compare the EL imaging with the LBIC measurement and explain how the images relate with the local quantum efficiency. Finally, we discuss how the quality of any diode used as an LED depends on its open circuit voltage if operated as a solar cell.

Acknowledgements

The authors would like to thank J. Mattheis, P. P. Altermatt, R. Brendel, for fruitful discussions and P. J. Rostan for fabricating the solar cells.

REFERENCES

1. Trupke T, Bardos R, Schubert MC, Warta W. Photoluminescence imaging of silicon wafers. *Applied Physics Letters* 2006; **89**: 044107-1-3.
2. Fuyuki T, Kondo H, Yamazaki T, Takahashi Y, Uraoka Y. Photographic surveying of minority carrier diffusion length in polycrystalline silicon solar cells by electroluminescence. *Applied Physics Letters* 2005; **86**: 262108-1-3.
3. Rau U. Reciprocity relation between photovoltaic quantum efficiency and electroluminescent emission of solar cells. *Physical Review B* 2007; **76**: 085303-1-8.
4. Ramspeck K, Bothe K, Hinken D, Fischer B, Schmidt J, Brendel R. Recombination current and series resistance imaging of solar cells by combined luminescence and lock-in thermography. *Applied Physics Letters* 2007; **90**: 153502-1-3.
5. Würfel P, Trupke T, Puzzer T, Schäffer E, Warta W, Glunz SW. Diffusion lengths of silicon solar cells from luminescence images. *Journal of Applied Physics* 2007; **101**: 123110-1-10.
6. Kirchartz T, Helbig A, Rau U. Quantification of light trapping using a reciprocity between electroluminescent emission and photovoltaic action in a solar cell. *Materials Research Society Symposium Proceedings*. San Francisco: 2008, 1101-KK 01-04 (MRS, Warrendale, PA, 2008).
7. Kirchartz T, Rau U, Kurth M, Mattheis J, Werner JH. Comparative study of electroluminescence from Cu(In,-Ga)Se_2 and Si solar cells. *Thin Solid Films* 2007; **515**: 6238–6242.
8. Kirchartz T, Rau U. Electroluminescence analysis of high efficiency Cu(In,Ga)Se_2 solar cells. *Journal of Applied Physics* 2007; **102**: 104510-1-8.

DOI: 10.1002/pip

9. Kirchartz T, Rau U, Hermle M, Bett AW, Helbig A, Werner JH. Internal voltages in GaInP/GaInAs/Ge multijunction solar cells determined by electroluminescence measurements. *Applied Physics Letters* 2008; **92**: 123502-1-3.
10. Green MA. *Solar Cells, Operating Principles, Technology and System Applications*. University of New South Wales: Sydney, 1986; 92–98.
11. Donolato C. A reciprocity theorem for charge collection. *Applied Physics Letters* 1985; **46**: 270–272.
12. Kerr MJ, Cuevas A. General parameterization of Auger recombination in crystalline silicon. *Journal of Applied Physics* 2002; **91**: 2473–2480.
13. Yablonovitch E. Statistical ray optics. *Journal of the Optical Society of America* 1982; **72**: 899–907.
14. Brendel R. Coupling of light into mechanically textured silicon solar cells—a ray tracing study. *Progress in Photovoltaics: Research and Applications* 1995; **3**: 25–38.
15. Hinken D, Ramspeck K, Bothe K, Fischer B, Brendel R. Series resistance imaging of solar cells by voltage dependent electroluminescence. *Applied Physics Letters* 2007; **91**: 182104-1-3.
16. Kirchartz T, Helbig A, Rau U. Note on the interpretation of electroluminescence images using their spectral information. *Solar Energy Materials and Solar Cells* 2008; **92**: 1621–1627.
17. Tiedje T, Yablonovitch E, Cody GC, Brooks BG. Limiting efficiency of silicon solar cells. *IEEE Transactions on Electronic Devices* 1984; ED-31: 711–716.
18. Trupke T, Daub E, Würfel P. Absorptivity of silicon solar cells obtained from luminescence. *Solar Energy Materials and Solar Cells* 1998; **53**: 103–114.
19. Taguchi M, Terakawa A, Maruyama E, Tanaka M. Obtaining a higher Voc in HIT cells. *Progress in Photovoltaics: Research and Applications* 2005; **13**: 481–488.
20. Green MA, Zhao J, Wang A, Reece PJ, Gal M. Efficient silicon light-emitting diodes. *Nature* 2001; **412**: 805–808.

DOI: 10.1002/pip